Cell Metabolism
Article

# A SPAK Isoform Switch Modulates Renal Salt Transport and Blood Pressure

James A. McCormick,[1,5,*] Kerim Mutig,[2,5] Joshua H. Nelson,[1,5] Turgay Saritas,[2] Ewout J. Hoorn,[1] Chao-Ling Yang,[1] Shaunessy Rogers,[1] Joshua Curry,[1] Eric Delpire,[3] Sebastian Bachmann,[2] and David H. Ellison[1,4]
[1]Division of Nephrology and Hypertension, Oregon Health and Science University, Portland, OR 97239-3098, USA
[2]Institut für Vegetative Anatomie, Charité-Universitätsmedizin Berlin, Campus Charité-Mitte, 10115 Berlin, Germany
[3]Vanderbilt University, Nashville, TN 37240, USA
[4]VA Medical Center, Portland, OR 97239, USA
[5]These authors contributed equally to this work
*Correspondence: mccormij@ohsu.edu
DOI 10.1016/j.cmet.2011.07.009

## SUMMARY

**The renal thick ascending limb (TAL) and distal convoluted tubule (DCT) play central roles in salt homeostasis and blood pressure regulation. An emerging model suggests that bumetanide- and thiazide-sensitive NaCl transporters (NKCC2 and NCC) along these segments are phosphorylated and activated by WNK kinases, via SPAK and OSR1. Here, we show that a kidney-specific SPAK isoform, which lacks the kinase domain, inhibits phosphorylation of NCC and NKCC2 by full-length SPAK in vitro. Kidney-specific SPAK is highly expressed along the TAL, whereas full-length SPAK is more highly expressed along the DCT. As predicted from the differential expression, SPAK knockout in animals has divergent effects along TAL and DCT, with increased phosphorylated NKCC2 along TAL and decreased phosphorylated NCC along DCT. In mice, extracellular fluid volume depletion shifts SPAK isoform abundance to favor NaCl retention along both segments, indicating that a SPAK isoform switch modulates sodium avidity along the distal nephron.**

## INTRODUCTION

Arterial pressure and extracellular fluid (ECF) volume are determined largely by renal NaCl excretory capacity. A key signaling pathway that modulates NaCl reabsorption and $K^+$ secretion involves WNK kinases interacting with SPAK and OSR1. These kinases act along the distal nephron to modulate the bumetanide-sensitive Na-K-2Cl cotransporter (NKCC2) and the thiazide-sensitive NaCl cotransporter (NCC). The STE20 (sterile 20)-like kinases SPAK (STE20- and SPS1-related proline/alanine-rich kinase) and OSR1 (oxidative stress response kinase-1, abbreviated *OXSR1* in GenBank) contribute to ion homeostasis and cell volume control (Delpire and Gagnon, 2008). In mammalian cells, SPAK phosphorylates and activates the cation chloride cotransporters, NKCC1, NKCC2, and NCC, under hyperosmotic or hypotonic low-$Cl^-$ conditions (Richardson et al., 2011); members of the WNK family act upstream of SPAK, phosphorylating it within the T-loop of the catalytic domain and within a C-terminal noncatalytic region (Vitari et al., 2005). WNK kinase effects on SPAK activity may contribute to human hypertension, as mutations in genes encoding WNK 1 and 4 cause the human disease familial hyperkalemic hypertension (FHHt, also known as pseudohypoaldosteronism II, or Gordon Syndrome) (Wilson et al., 2001), a disease associated with increased NCC activity (Mayan et al., 2002).

These data have led to a linear model of WNK/SPAK-OSR1/NKCC2-NCC signaling in which WNKs phosphorylate and activate SPAK-OSR1, which phosphorylates and activates NCC and NKCC2 (Richardson and Alessi, 2008). This suggests that SPAK-OSR1 inhibition should suppress the activity of both NCC and NKCC2 (Richardson et al., 2011). Yet recent data from animal models are not entirely consistent with this view. Alessi and colleagues (Rafiqi et al., 2010) generated mice that express a SPAK mutant that cannot be activated. The animals exhibited reductions in phosphorylated (activated) NCC and NKCC2 and were substantially hypotensive. In contrast, Yang and colleagues reported that, in SPAK knockout animals, there was less phosphorylated NCC, but more phosphorylated NKCC2 in kidney; the salt-wasting phenotype in these mice was also milder. Thus, deletion of SPAK and inactivation of SPAK have similar effects on NCC, but divergent effects on NKCC2; this discrepancy was pointed out recently in an editorial (Rodan and Huang, 2010). Here, we show that renal SPAK comprises several structurally and functionally dissimilar isoforms, at least one of which is inhibitory rather than stimulatory. These isoforms are differentially expressed along the TAL and DCT and are regulated according to ECF volume. The data provide an explanation for the discrepant results described above; suggest a reason that two very similar kinases, OSR1 and SPAK, are present in the same kidney epithelial cells; and unravel a mechanism for NaCl and blood pressure homeostasis.

## RESULTS

### Renal SPAK Products Include Antagonistic Isoforms

Typically, SPAK is believed to be a full-length kinase (Delpire and Gagnon, 2008), but additional forms have been described (Piechotta et al., 2003). Full-length SPAK is expressed prominently in brain and most other tissues (Rafiqi et al., 2010); on immunoblots from kidney, however, nearly all SPAK runs as

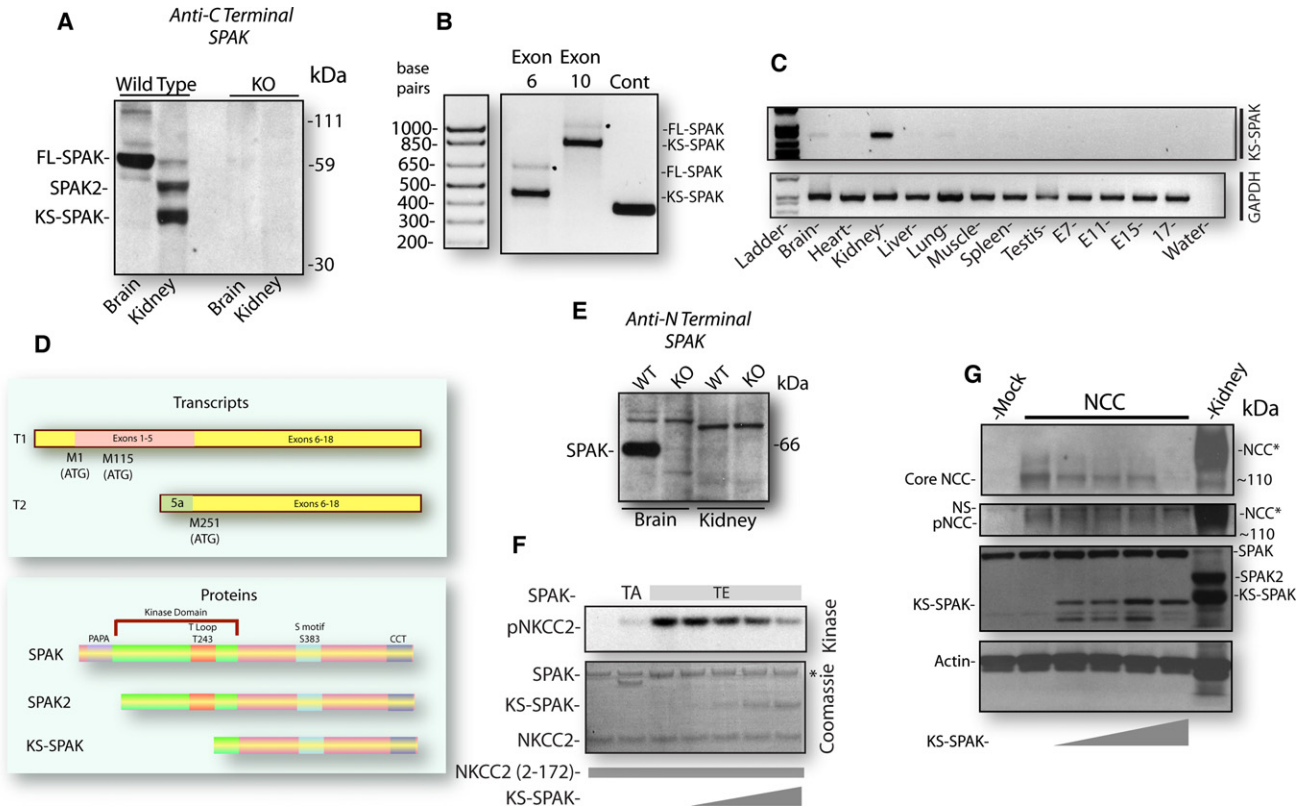


**Figure 1. Characterization of SPAK Isoforms**

(A) Immunoblot of mouse kidney and brain, probed with an anti-SPAK antibody recognizing a carboxyl-terminal domain. Brain SPAK runs predominantly near 59 kDa, whereas kidney SPAK runs primarily as two smaller bands, labeled SPAK2 and KS-SPAK. Tissue from SPAK knockout (KO) animals (see Figure 3) is shown as a control.

(B) 5′ RACE, using primers directed to exon 6 and 10. Note faint bands running as expected for full-length SPAK and dark bands running representing KS-SPAK. A positive control (Cont) is also shown.

(C) RT-PCR on a multitissue panel (E, whole embryo), using forward primer to exon 5a and reverse primer to exon 10, shows that KS-SPAK expression is almost exclusively restricted to kidney. GAPDH serves as a positive control and water as a negative control.

(D) Top panel shows transcripts showing the alternative translation initiation sites (top) and the alternative transcript showing exon 5a and the third ATG (bottom). Bottom panel shows protein products derived from these transcripts, including the PAPA box, and the kinase domain, with T243 within the T loop, the S motif, and the CCT domain.

(E) Immunoblot of brain and kidney probed with an anti-N-SPAK antibody. Tissue from SPAK KO mice (see Figure 3) is included as a control. Note the faint band in WT kidney. Other bands are nonspecific, as indicated by their presence in the KO animals.

(F) In vitro kinase assay; NKCC2 was incubated with low-activity SPAK (T243A) or constitutively active SPAK (T243E). Effects of increasing KS-SPAK (triangle) on SPAK-dependent NKCC2 phosphorylation (pNKCC2) are shown. Coomassie (lower panel) shows protein products, with * indicating that a contaminant (appearing even in the first lane, when SPAK was not added) runs at the same apparent size as SPAK. Note that inactive SPAK T243A (TA) migrates at a different size compared with constitutively active SPAK T243E (TE).

(G) Kinase activity in HEK cells transfected with NCC. Increasing KS-SPAK (triangle) decreases total and phosphorylated NCC. Phosphorylated NCC from cells is the diffuse band (pNCC, not the nonspecific band, NS). Note that KS-SPAK runs as a doublet, suggesting posttranslational modification. Kidney tissue is shown at the right, with fully glycosylated, mature NCC marked with *.

smaller products (Rafiqi et al., 2010). Furthermore, SPAK precipitated from kidney is largely devoid of kinase activity (Rafiqi et al., 2010). Here (Figure 1A), we confirmed that SPAK in brain runs as expected for the full-length product (~60 kDa), whereas kidney SPAK runs primarily as faster-migrating bands. Piechotta and colleagues (Piechotta et al., 2003) showed that SPAK can be generated from two translation initiation sites, one 115 base pairs downstream from the full-length SPAK START codon. This smaller product lacks the entire PAPA box and was predicted to be kinase defective (Piechotta et al., 2003); we term it SPAK2. Immunoblots from kidney and other tissues show a band of a size near to that predicted for the second translation initiation site (Figure 1A) (Rafiqi et al., 2010). In addition, however, a smaller band appears prominently in kidney (Figure 1A); this band has not been observed in other tissues (Figure 1A) (Rafiqi et al., 2010).

Our observation of at least three SPAK products on renal immunoblots suggested the existence of either yet another alternative translation START or a splice variant. To address this possibility, we performed 5′ and 3′ RACE, using total RNA from mouse kidney. The major product identified in kidney corresponded to a transcript that differs from that predicted for the full-length SPAK, which was a minor amplified product (Figure 1B). The smaller transcript was isolated using primers

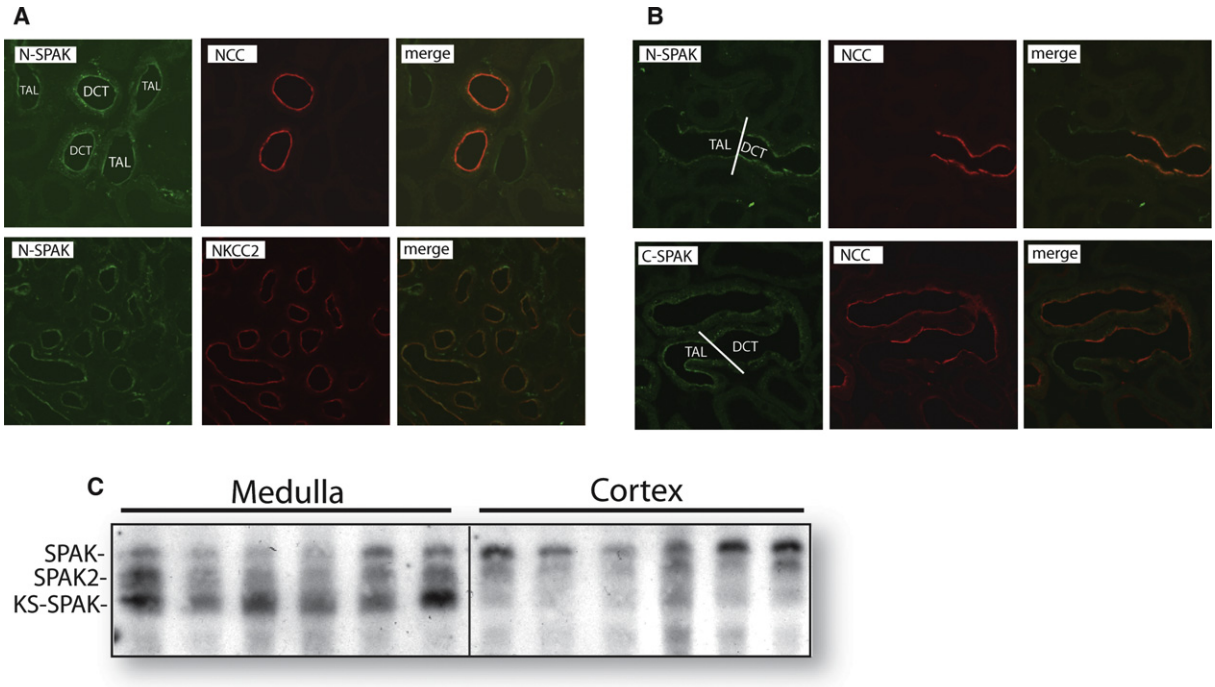


**Figure 2. Sites of SPAK Expression in Kidney**

(A) SPAK (here detected with an anti-N-SPAK antibody) is expressed along both the TAL and the DCT, as indicated by colocalization with NCC and anti-NKCC2.

(B) Sites of expression of full-length SPAK (detected with anti-N-SPAK) and total SPAK (detected with anti-C-SPAK). Transitional segments containing both TAL and DCT are shown, as determined using anti-NCC and anti-NKCC2 antibodies. Note that full-length SPAK expression is higher along DCT than TAL, whereas total SPAK expression is higher along TAL than DCT.

(C) Total SPAK immunoblot of medullary and cortical tissue. Note that most cortical SPAK is the full-length isoform (SPAK), whereas KS-SPAK and SPAK2 are more highly expressed in medulla.

targeting both exons 6 and 10 and contained a distinct first exon (exon 5a, see Figure S1 for sequence), located within intron 5–6, about 17 kb upstream of exon 6, in the genomic sequence. The same transcript has been identified previously as an expressed sequence tag (EST) in mouse mammary tumor (NCBI accessions BL110429.1 and AQ988594.1), but based on western blotting data (Rafiqi et al., 2010), its expression pattern appears largely restricted to kidney. To confirm this, we performed RT-PCR using primers specific for the novel transcript-specific exon 5a and the shared exon 10. As shown in Figure 1C, the transcript was not detected at substantial levels in other tissues; thus, we have termed it kidney-specific SPAK (KS-SPAK) (GenBank accession JN368425). Seven out-of-frame START codons are present in exons 5a and 6 prior to the first in-frame START (equivalent to M251 in full-length SPAK), so the proposed protein does not contain any novel amino acid sequence, but is rather a truncation of full-length SPAK (Figure 1D).

Both KS-SPAK and SPAK2 are predicted to lack the N terminus (Figure 1D), which is present in the full-length protein. To confirm the identity of these products, we used antibodies directed against the SPAK N terminus. Figure 1E confirms that full-length SPAK, but not SPAK2 or KS-SPAK, is recognized by the antibody directed toward an amino-terminal epitope. Full-length SPAK is prominent in the brain (and other tissues, data not shown); in kidney, however, its abundance is substantially lower. Thus, much of renal SPAK lacks an amino terminus. When apparent molecular weights were examined at higher resolution (Figure S2), the three renal SPAK forms ran somewhat larger than their predicted sizes. Furthermore, when expressed in HEK293 cells by transfection, the three SPAK isoforms ran close to, but not precisely at, the sizes observed in kidney. These data suggest that SPAK isoforms undergo significant posttranslational modification in vivo.

KS-SPAK retains its conserved C-terminal (CCT) domain, which has been shown to bind to NKCC2, to participate in phosphorylation and activation (Richardson et al., 2011). Furthermore, synthetic kinase-dead SPAK mutants exhibit dominant-negative effects on wild-type (WT) SPAK (Dowd and Forbush, 2003). Thus, we tested whether KS-SPAK might inhibit SPAK activity; in vitro, KS-SPAK inhibited phosphorylation of both NKCC2 and NCC by SPAK, rendered constitutively active (T243E), in a dose-dependent manner (Figures 1F and S3). To confirm the relevance of this observation in mammalian tissue, we used HEK293 cells, which express SPAK primarily as the kinase-active full-length form (see Figure 1G). The cells were transfected with both NCC and KS-SPAK. Cotransfection with KS-SPAK led not only to a dose-dependent decrease in phosphorylated NCC, but also to a substantial decrease in total NCC abundance. (Figure 1G).

## SPAK Isoforms Are Differentially Expressed along TAL and DCT

Figure 2A shows that SPAK is expressed along both the DCT and the TAL, where it colocalizes with both NCC and NKCC2;

expression was not detected in other segments. To determine whether the full-length SPAK is expressed equally along TAL and DCT, additional immunofluorescence compared transitional nephron segments, using both anti-N-SPAK and anti-C-SPAK antibodies. Figure 2B shows that full-length SPAK is modestly expressed along the TAL, but is more apparent along the DCT. In contrast, total SPAK (comprising both full-length and truncated forms and detected using the anti-C-SPAK antibody) appears to be much more abundant along the TAL than the DCT. Immunofluorescence is not quantitative, so we examined immunoblots of kidney cortex and medulla. We reasoned that medulla contains only TAL, whereas cortex contains both DCT and TAL. Figure 2C shows striking differences in SPAK isoform expression; in cortex, SPAK is predominantly full length, whereas in medulla, most SPAK is SPAK2 and KS-SPAK. Together, these data suggest that SPAK along the DCT should stimulate NCC transport, as the full-length, kinase-active form predominates. In contrast, SPAK along the TAL should be inhibitory, as the predominant forms lacking the kinase domain can inhibit SPAK activity.

## SPAK Knockout Mice Display Salt-Sensitive Hypotension and Electrolyte Imbalance

To test the hypothesis that SPAK forms exert opposite effects on cation chloride cotransporter activity along the TAL and DCT, we used SPAK knockout mice (Delpire and Gagnon, 2008; Geng et al., 2010). Due to the strategy used to generate them, SPAK$^{+/-}$ mice (referred to hereafter as heterozygotes, or HETs) cannot be distinguished from SPAK$^{-/-}$ mice (referred to hereafter as knockouts, or KOs) by PCR. Thus, we used all offspring obtained from HET intercrosses and performed phenotypic identification after completion of experimental maneuvers. The genotypes of WT, HET, and KO mice were verified using PCR, western blotting, and immunofluorescence (Figures 3A and 3B).

To determine the role of SPAK in blood pressure regulation, systolic blood pressure was measured by volume pressure-recording tail plethysmography (Feng et al., 2008). When consuming a control NaCl diet (0.49% NaCl), blood pressures of the three groups did not differ (Figure 3C). Dietary NaCl restriction (0.01% NaCl) for 7 days, however, reduced systolic pressure significantly in SPAK KO mice ($-9.4 \pm 2.1$ mm Hg), but not in WT and HET mice (Figure 3C).

To characterize electrolyte and renin-angiotensin-aldosterone system (RAAS) status, whole blood from WT, HET, and KO mice maintained on a standard diet was collected and immediately analyzed using an iSTAT blood chemistry analyzer (Table S1). Compared with WT mice, KO mice did not display any significant differences in whole blood electrolyte levels. In KO mice, however, there was a trend toward hypokalemia (WT, 4.6 mmol/l versus KO, 4.2 mmol/l) and hypomagnesemia (WT, 0.96 mmol/l versus KO, 0.88 mmol/l). As expected, plasma renin activity (PRA) was higher in KO than in WT mice, but aldosterone levels were not (see Discussion). Finally, SPAK KO mice were hypocalciuric, as shown by a significantly lower urinary calcium: creatinine ratio than WT mice (WT, $0.52 \pm 0.09$ mg/mg versus KO, $0.20 \pm 0.04$, $p < 0.05$) (see also Table S1). HETs were also significantly hypocalciuric ($0.29 \pm 0.06$, $p < 0.05$) compared with WT mice.

Mice were next subjected to manipulation of dietary electrolytes to aid identification of differences that were not apparent on a standard diet. Severe restriction of dietary $K^+$ resulted in dramatic reductions in whole blood $K^+$ in both WT and KO mice (data not shown), so a more modest restriction was performed (from 0.8% $K^+$ to 0.08% $K^+$). On this diet, whole blood $K^+$ was significantly lower in KO mice compared with WT mice (Figure 3D). Hypocalciuria owing to NCC deletion or inhibition has been proposed to result primarily from depletion of the ECF volume (Nijenhuis et al., 2005). To determine whether dietary NaCl loading could overcome the hypocalciuric effects of SPAK deletion, mice were salt loaded. In SPAK KO mice, urinary calcium/creatinine remained lower, compared with WT mice, even though urinary salt excretion rose to high levels, confirming that the ECF volume was expanded; HETs displayed an intermediate response (Figure 3E). PRA was significantly higher in KO mice on both normal and low-NaCl diet (Figure 3F). SPAK KO mice displayed a normal stimulation of aldosterone secretion in response to sodium restriction, but did not display a reduction in response to salt loading (Figure 3G).

## SPAK Deletion Stimulates NKCC2, but Inhibits NCC

To determine whether SPAK KO mice display abnormalities in NKCC2 or NCC expression and activity, we performed immunoblot analysis of protein lysates from WT, HET, and SPAK KO mice. On a standard NaCl diet, total NKCC2 expression did not differ between WT and SPAK KO mice (Figures 4A and 4B), but phosphorylated NKCC2 was increased substantially in the SPAK KO animals (Figures 4A and 4B). These data were confirmed by immunohistochemistry, which showed a marked increase in phosphorylated NKCC2 abundance in SPAK KO animals (Figure 4C).

In contrast, total NCC expression in SPAK KO mice was dramatically reduced (by 90% versus WT mice) on a standard NaCl diet (Figures 4D and 4E). To assess NCC activation status, we examined phosphorylation at T53 (and, in some studies, S71); the reduction in total NCC expression was matched by a similar decrease in phosphorylated NCC (Figures 4D and 4E). While HETs displayed a reduction in total NCC, phosphorylated NCC was essentially normal, indicating a compensatory effect in HETs (Figures 4D and 4E). Even after dietary salt restriction (0.01% NaCl), the abundance of phosphorylated NCC remained substantially reduced in SPAK KO animals (Figures 4D and 4E).

Yang and colleagues (Yang et al., 2010) reported that SPAK KO mice exhibit substantial reductions in natriuretic response to thiazides, with a preserved response to loop diuretics. To confirm those results and test whether changes in NKCC2 and NCC abundance and phosphorylation have functional consequences, the acute urinary $Na^+$ excretion in response to furosemide or hydrochlorothiazide (HCTZ) injection was determined. At baseline, urinary $Na^+$ excretion during 3 hr was similar in WT, HET, and SPAK KO mice (Table S1). Compared with WT animals, the natriuretic response to furosemide was increased in the SPAK KO animals, whereas the HCTZ response was reduced (Figure 4F); thus, the ratio of furosemide/HCTZ-induced natriuresis was significantly higher in the SPAK KO animals compared with WT animals ($p < 0.05$), consistent with the changes in phosphorylated NKCC2 and NCC.

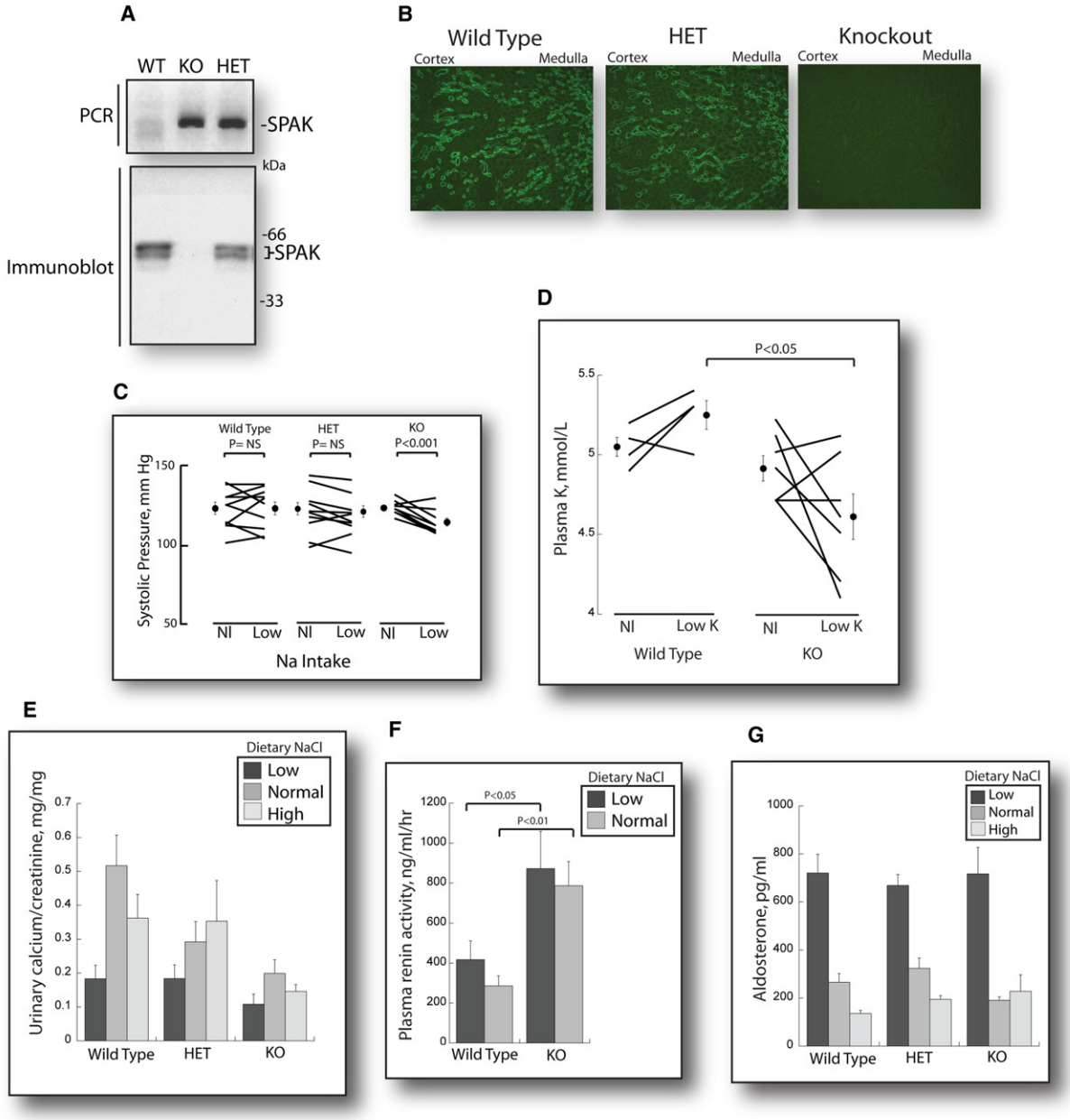


**Figure 3. Targeted Disruption of SPAK and SPAK Isoforms**

(A) PCR and immunoblot analysis to identify WT, HET, and KO mice. In this low-penetrated blot, full-length SPAK is not evident.

(B) Immunofluorescent analysis of kidney sections revealed expression of SPAK in WT and HET mice and confirmed ablation of SPAK in SPAK KO mice.

(C) Systolic blood pressure on normal- (Nl) NaCl intake diet (0.49% NaCl) and after 10 days on a low-NaCl intake diet (0.01% NaCl). Data are plotted as lines for individual mice on each diet; the mean systolic pressures ± SEM are shown as closed circles. Systolic pressure was reduced in SPAK KO mice (Mann-Whitney test) after NaCl restriction.

(D) On a normal- (Nl) $K^+$ intake diet (0.8% $K^+$), whole blood $K^+$ did not significantly differ between WT and KO mice. Whole blood $K^+$ was significantly lower in SPAK KO mice on a $K^+$-restricted diet than in WT mice (Mann-Whitney test). Values here are slightly higher than in Table S1, as the blood was obtained here by saphenous puncture rather than cardiac puncture. Data are plotted as above.

(E) Effects of dietary NaCl intake on urinary calcium excretion, expressed as the ratio of calcium to creatinine. Data are mean ratio ± SEM, n = 8–14.

(F) Plasma renin activity (PRA) in SPAK KO mice on both low- and normal-NaCl-intake diets. Data are mean ± SEM, n = 4–6.

(G) Effects of SPAK KO and of dietary NaCl on aldosterone. Data are mean ± SEM n = 8–10 on normal-NaCl intake, 5–7 on high NaCl intake, and 5 WT, 6 KO, and 13 HETs on low-NaCl intake.

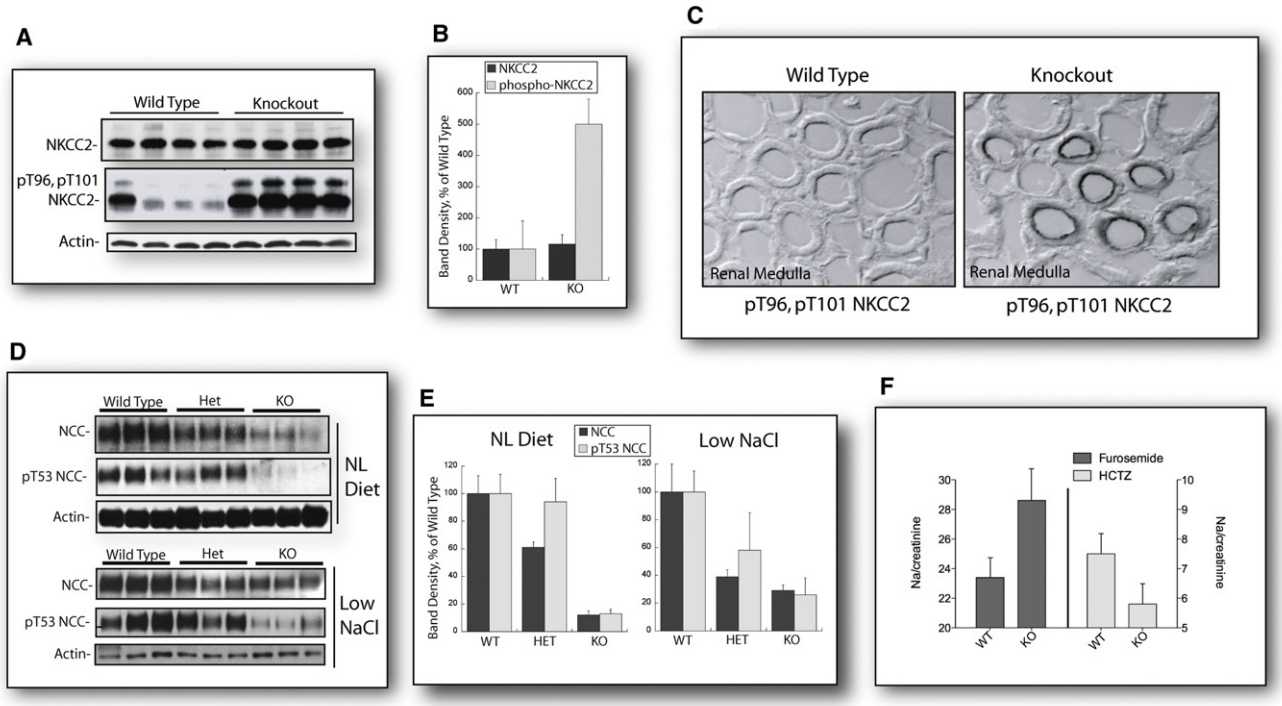


**Figure 4. SPAK Deletion Increases Phosphorylated NKCC2 and Decreases Phosphorylated NCC**

(A) Western blotting of kidney protein lysates revealed no change in total expression of NKCC2, but increased expression of phospho-NKCC2 (pT96, pT101) in SPAK KO mice.

(B) Densitometry revealed that SPAK KO mice display a 4-fold increase in phospho-NKCC2 levels (±SEM, n = 4, $p < 0.001$, Mann-Whitney test).

(C) This was also apparent on immunofluorescent analysis of kidney.

(D) Total and p-NCC (pT53) expression is reduced in NCC KO mice on normal and low-salt diet.

(E) Total and p-NCC (±SEM) were reduced by 90% relative to β-actin (n = 3, $p < 0.05$ versus WT, Mann-Whitney test). Similar results were seen in salt-deprived animals.

(F) Natriuretic effects (±SEM) of furosemide tended to be greater, and of hydrochlorothiazide (HCTZ) less, in KO compared to WT mice. The differential response between groups was significant. (n = 6 and 5 in WT and KO, $p < 0.05$, Mann-Whitney test.)

## SPAK Deletion Reduces DCT Mass, but Does Not Shift NCC from the Apical Membrane

To determine whether SPAK KO reduced NCC at the apical membranes preferentially, kidney sections were examined by immunofluorescence and by immunogold electron microscopy. The results confirmed that SPAK KO reduced total NCC abundance, as well as the abundance of NCC phosphorylated at T53 and S71 (Figures 5A and 5B). Despite the reduction, both total and phosphorylated NCC remained predominantly at the apical membrane; SPAK KO did not lead to an intracellular shift (Figure 5C). Apical expression is clearly a requirement for NCC to transport NaCl into the cell; these data suggest that NCC trafficking to and residence in the plasma membrane is not affected substantially by SPAK phosphorylation, a finding consistent with in vitro data (Glover et al., 2009). Even in the SPAK KO animals, phosphorylated NCC was restricted to the apical membrane and did not appear in intracellular vesicles (Figure 5D).

Low-power immunohistochemistry suggested that the number of DCT profiles is reduced in SPAK KO mice (Figure 5E). Quantitative analysis confirmed that the fractional DCT volume (determined as the fraction of tubules that express NCC) is approximately 50% lower in SPAK KO mice compared to WT (Figure 5F). Thus, a substantial portion of the reduction in total and phosphorylated NCC reflects underdevelopment of the DCT.

## OSR1 Expression Is Maintained in SPAK KO Animals

The observation that deletion of SPAK increases NKCC2 phosphorylation suggests that SPAK (presumably KS-SPAK) along the TAL is inhibiting a kinase at baseline, yet the kinase cannot be SPAK alone, as NKCC2 phosphorylation is increased even though all SPAK is absent. OSR1 and SPAK share the ability to phosphorylate cation chloride cotransporters, and both proteins are expressed in kidney (Rafiqi et al., 2010). To confirm that OSR1 expression patterns mirror those of SPAK, we examined OSR1 abundance in WT and SPAK KO animals by immunofluorescence. The results confirm that OSR1 is expressed along the TAL (Figure 6A) and DCT (Figure 6B) in a distribution resembling that of SPAK. OSR1 expression was not affected substantially by SPAK deletion (Figure 6C); it remained predominantly near the apical membrane, close to NCC and NKCC2 (Figures 6A and 6B). Of note, in DCT profiles of SPAK KO mice, OSR1 did exhibit a more punctate distribution than it did in WT animals. We also confirmed (Figure 6C) the observation of Yang and colleagues (Yang et al., 2010) that the abundance of phosphorylated OSR1 is increased by SPAK KO (approximately

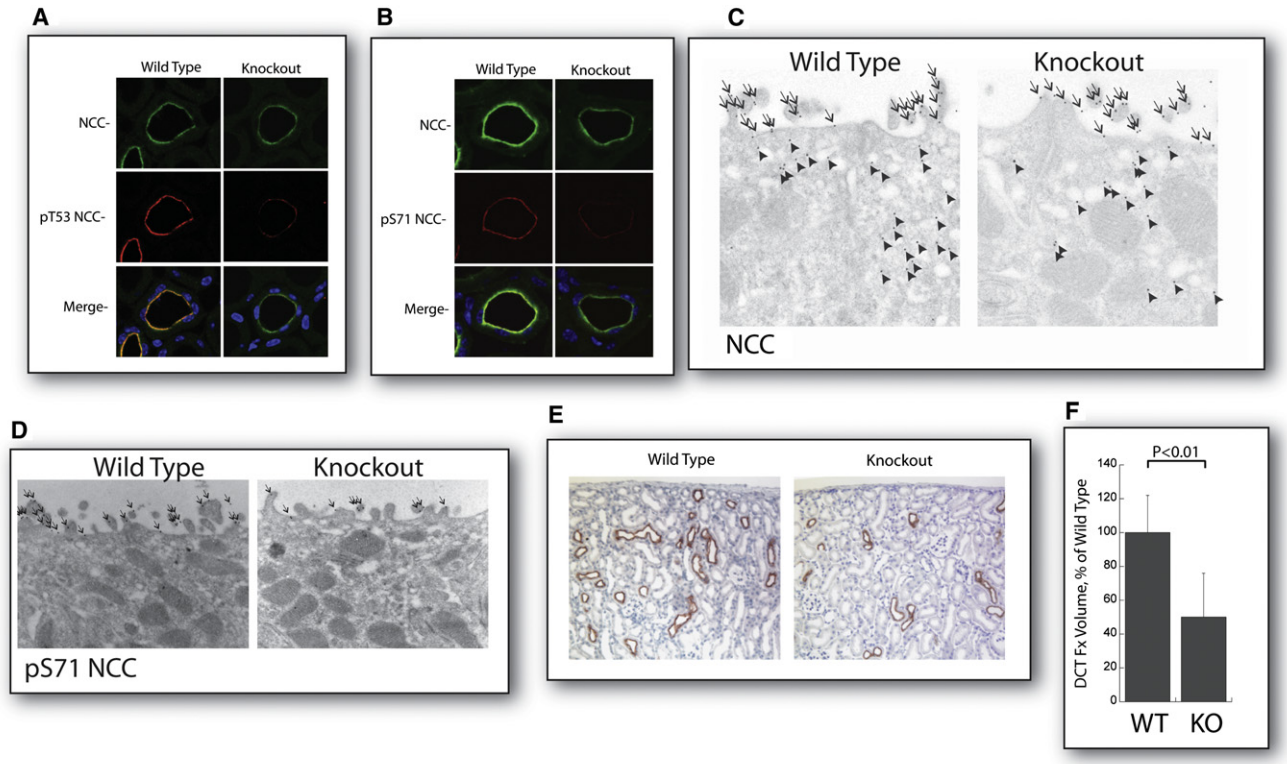


**Figure 5. Apical Membrane Localization of NCC Is Unchanged in SPAK KO Mice, but Fractional Volume of the DCT Is Reduced**

(A and B) Immunofluorescence on kidney sections using antibodies against total NCC (A and B), pT53 NCC (A), and pS71 NCC (B) revealed that total and p-NCC apical membrane distribution is not altered in SPAK KO mice, despite a 90% reduction in total and p-NCC expression levels.

(C and D) Immunogold electron microscopy against total and p-NCC revealed that the relative abundance of total NCC (C) and pS71 (D) in the apical membrane versus inside of cells was not altered by SPAK KO. Note that while total NCC is detected at both apical and subapical regions, pS71 NCC is expressed only on the apical surface. Arrows indicate apical localization, and arrowheads indicate subapical localization.

(E) Low-power images of kidney sections stained for NCC expression (brown staining) by immunohistochemistry suggest fewer DCT segments.

(F) Quantification of the fractional volume of the DCT (DCT Fx volume) confirmed a 54% reduction in DCT in SPAK KO mice (mean ± SEM, n = 4).

2× that of WT, p = 0.01). Together, these results suggest that an important function of KS-SPAK along the TAL is to inhibit OSR1. In support of this model, we found that KS-SPAK is capable of inhibiting the ability of OSR1 to phosphorylate NKCC2 in vitro (Figure 6D).

### Extracellular Volume Depletion Generates a SPAK Isoform Switch

We next tested the hypothesis that dietary NaCl intake alters the relative abundance of SPAK products. Figure 7A shows that dietary NaCl restriction reduced the abundance of KS-SPAK (the inhibitory form) while increasing the abundance of longer (presumably stimulatory) forms. Further, the activated SPAK isoforms shifted to a higher apparent molecular weight, an effect described previously (Anselmo et al., 2006). It should also be noted that additional, undefined forms of SPAK appeared following dietary NaCl restriction. These results suggested that mild depletion of the ECF volume, as induced by dietary restriction, was sufficient to effect this change. We confirmed this hypothesis by comparing NCC KO animals with their WT controls. Figure 7B shows that NCC KO animals exhibit a similar SPAK isoform shift compared with their WT controls (quantified in Figure S4). The animals also exhibit an increase in total and phosphorylated NKCCs (Figure S5). In contrast, the pattern and abundance of OSR1 do not appear to be affected by NCC KO (Figure 7C).

## DISCUSSION

SPAK, OSR1, and the WNK kinases interact in the distal nephron to regulate NCC and NKCC2 activity, modulating salt and potassium balance and arterial pressure. While it is now clear that WNK kinases can phosphorylate and activate both SPAK and OSR1 and that SPAK and OSR1 can activate and phosphorylate NCC and NKCC2 (Richardson and Alessi, 2008), there is less information about how these kinases interact to regulate salt transport in animals. Here, we identified interactions between previously unrecognized SPAK isoforms that modulate NCC and NKCC2 in vivo. We determined that a KS-SPAK isoform exerts inhibitory rather than stimulatory effects on NaCl transport both in vitro and in vivo. Further, we show that loss of this isoform accounts for the anomalous effects of SPAK KO on NKCC2 activity. Finally, we showed that SPAK isoform abundance is subject to substantial regulatory modulation; together, these proteins form a WNK/SPAK-OSR1 signaling complex in the distal nephron.

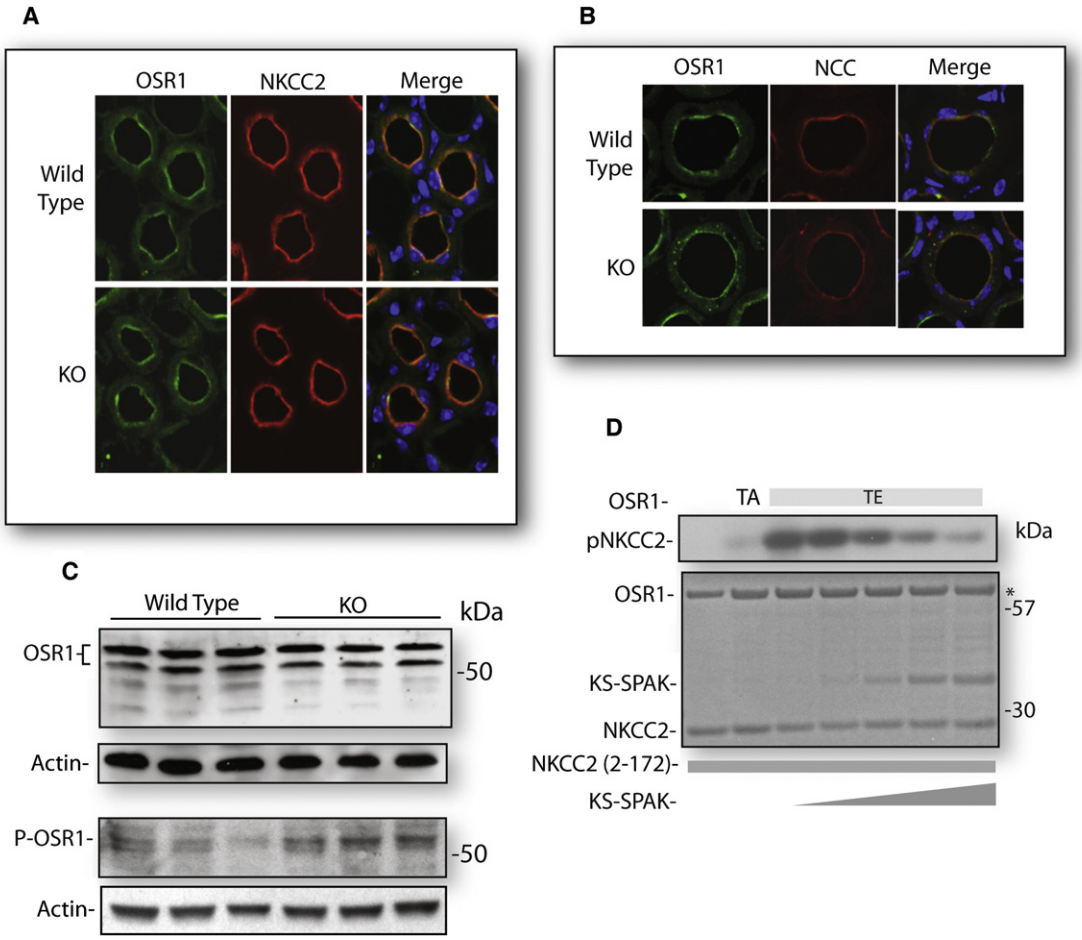


**Figure 6. Distribution and Expression of OSR1 in SPAK KO Mice**

(A) OSR1, expressed along the TAL with NKCC2, is not affected by SPAK KO.

(B) OSR1 also expressed along the DCT with NCC; in SPAK KO mice, OSR1 expression appeared more punctuate than in WT mice.

(C) Immunoblot analysis of total expression of OSR1 revealed no substantial difference between WT and SPAK KO mice. Bottom panel shows, however, that phosphorylated OSR1 was increased by SPAK KO (216% in SPAK KO, n = 3, p = 0.01).

(D) In vitro kinase assay; NKCC2 was incubated with low-activity OSR1 (T185A) or constitutively active OSR1 (T185E). Effects of increasing KS-SPAK (triangle) on OSR1-dependent NKCC2 phosphorylation (pNKCC2) are shown. Coomassie (below) shows protein products, with * representing a contaminant in the protein prep that was present even when OSR1 was not included (first lane). Note that when OSR1 is included, the band becomes darker and runs as a subtle doublet.

In vitro, SPAK can activate both NKCC2 and NCC by phosphorylating residues along their amino-terminal cytoplasmic domains; SPAK and OSR1, in turn, can be activated by several WNK kinases (Richardson and Alessi, 2008). Based upon these properties and the documented expression of SPAK along the TAL and DCT, it would be predicted that SPAK deletion should impair NaCl reabsorption along both nephron segments, generating a phenotype combining features of both Bartter and Gitelman syndromes. Two mouse models have been consistent with this view (Table S2). First, $SPAK^{T243A/T243A}$ knockin mice, which express a SPAK protein devoid of kinase activity, have lower arterial pressure and less phosphorylated NKCC2 and NCC than WT mice (Rafiqi et al., 2010). Second, mice deficient in SORLA (sorting-protein-related receptor with A-type repeats), which is expressed along the TAL and DCT, display a phenotype with features of mild type I Bartter Syndrome (in which NKCC2 has been disrupted), including excessive urinary $K^+$ and $Ca^{2+}$ excretion (Reiche et al., 2010). In SORLA KO mice, levels of total SPAK were unchanged, but SPAK shifted away from NKCC2 to a more subapical region with reductions in phosphorylated NKCC2.

In contrast, the results of Yang and colleagues (Yang et al., 2010) and the current results both show that SPAK KO increases the phosphorylation (and activity) of one transporter (NKCC2) while reducing the phosphorylation of the other (NCC). We considered several explanations to account for these differences. First, ECF volume depletion, owing to NCC inactivity, might have stimulated NKCC2 phosphorylation secondarily, independent of SPAK. Yet ECF volume depletion per se does not seem to be the dominant cause, as $SPAK^{T243A/T243A}$ mice, which exhibit the same or even greater ECF fluid volume depletion, display less, not more, phosphorylated NKCC2 (Rafiqi et al., 2010; Rodan and Huang, 2010). A second possibility was that SPAK deletion might somehow have led to compensatory

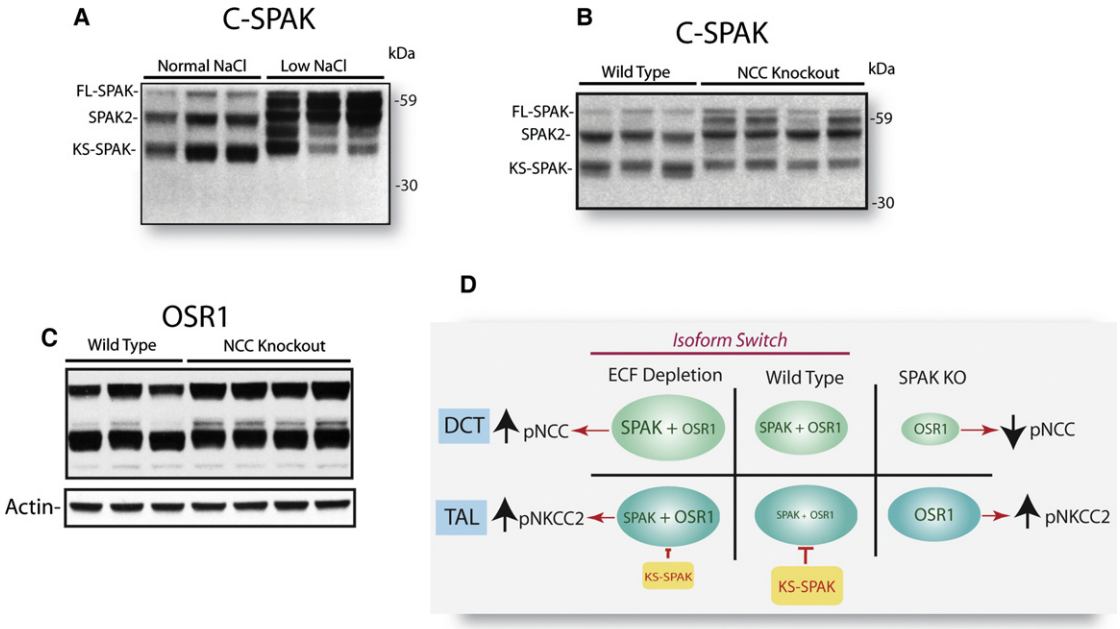


**Figure 7. SPAK Isoform Shift**

(A) C-SPAK immunoblot comparing WT mice on a normal and restricted-NaCl diet. Note the increase in KS-SPAK and SPAK2, the decline in KS-SPAK abundance, and the appearance of additional products.

(B) C-SPAK immunoblot comparing WT mice on a normal diet with NCC KO mice on a normal diet. Qualitatively similar changes as in (A) were observed.

(C) OSR1 immunoblot comparing WT mice and NCC KO mice, showing no changes comparable to those for SPAK.

(D) Model of SPAK and OSR1 actions along the distal nephron. Model is simplified by assuming that all SPAK in DCT is full length whereas most SPAK in TAL is truncated. Active kinases are labeled in green, while the inactive KS-SPAK is labeled in red. KS-SPAK in TAL inhibits SPAK and OSR1 in WT animals. SPAK KO leads to the changes in transport activity observed by removing active SPAK from DCT (decreasing NCC activity), but alleviating KS-SPAK inhibition of OSR in TAL (increasing NKCC2 activity). The model also shows how the SPAK isoform switch, induced by ECF depletion, stimulates transport along TAL and DCT by reducing the abundance of KS-SPAK in TAL, but increasing the abundance of active kinases in both segments. This model does not show phosphorylation of the kinases, but this is clearly an essential element of activation.

increases in OSR1 abundance along TAL. Figure 6 provides evidence that OSR1 abundance is not increased by SPAK deletion, a finding similar to that of Rafiqi and colleagues in SPAK$^{T243A/T243A}$ mice (Rafiqi et al., 2010). Thus, there is little evidence that SPAK deletion or inactivation itself increases the abundance of OSR1. A third possibility is that SPAK expressed by TAL cells acts to suppress rather than stimulate transport; we suggest that this inhibitory activity is mediated by KS-SPAK, as this isoform appears to be most abundant along this segment. Comparison of the current results with those derived from the SPAK$^{T243A/T243A}$ mice provides support for such a model (see Figure 7D). When SPAK kinase activity is disrupted but SPAK abundance is maintained (as in SPAK$^{T243A/T243A}$ mice), the balance between kinase-inactive SPAK and kinase-active SPAK reduces the abundance of phosphorylated NKCC2 (Rafiqi et al., 2010); when SPAK is deleted entirely, however, the inhibitory protein (KS-SPAK) is absent, and the abundance of phosphorylated NKCC2 rises (Yang et al., 2010). Deletion of KS-SPAK along the TAL increases OSR1 phosphorylation in vivo. We suggest that this occurs because KS-SPAK normally acts along the TAL to inhibit OSR1 phosphorylation (see Figure 6D).

This model (Figure 7D) also accounts for the effect of SPAK KO along the DCT, where decreased rather than increased NCC activity is observed. Along DCT, most SPAK appears to be kinase active (Figure 2); deleting it reduces NCC phosphorylation. As noted (Figure 7), ECF volume depletion shifts SPAK isoforms away from short products (such as KS-SPAK) and toward full-length products, favoring SPAK-mediated phosphorylation (Figure 7D); whether this shift occurs uniformly along the TAL and DCT remains to be established. Possible mediators of the switch include angiotensin II and arginine vasopressin (Mutig et al., 2010; van der Lubbe et al., 2011; Welker et al., 2008), but not aldosterone, as SPAK KO animals exhibit reduced plasma aldosterone levels. The reduced aldosterone levels may reflect SPAK-mediated regulation of aldosterone secretion, as adrenal glands express SPAK abundantly (Delpire and Gagnon, 2008).

This renal-specific expression of a kinase-deficient truncated product is strikingly reminiscent of the renal-specific expression of KS-WNK1, a kinase-defective WNK1 isoform, along the distal nephron that modulates NCC activity both in vitro (Subramanya et al., 2006) and in vivo (Hadchouel et al., 2010; Liu et al., 2009). This protein inhibits the kinase activity of WNK1 (Lazrak et al., 2006; Subramanya et al., 2006; Wade et al., 2006), acting as a molecular switch in the distal nephron. One interesting difference between KS-WNK1 and KS-SPAK is that the former appears to be modulated primarily by dietary KCl intake (Lazrak et al., 2006; Wade et al., 2006), whereas the latter is modulated strongly by ECF volume (Figure 7); although effects of KCl intake on KS-SPAK have yet to be tested directly, this raises the

possibility that interactions between WNK kinases and SPAK/OSR1 are instrumental in balancing NaCl and K excretion.

These data also illuminate mechanisms by which the WNK/SPAK/OSR1 signaling complex modulates NCC activity. To transport NaCl, NCC must be inserted into the apical membrane and also be phosphorylated (activated). In vitro, NCC trafficking can be dissociated from NCC phosphorylation (Glover et al., 2009), but the relationship between the two processes in vivo has remained obscure. There is strong evidence that NCC is inserted into and removed from the apical membrane in response to physiological need (Lee et al., 2009; Sandberg et al., 2006, 2007); as noted, there is also evidence that NCC phosphorylation can be regulated under many of the same circumstances. In the case of SPAK deletion, NCC remains predominantly apical, even though phosphorylation is largely abrogated by SPAK deletion; this result is reminiscent of the effects of SORLA KO on NKCC2; SORLA KO leads to a redistribution of SPAK away from the plasma membrane, but NKCC2 remains strictly apical. Thus, NCC activation likely reflects two distinct processes: trafficking to the apical membrane and activation by phosphorylation, perhaps within the apical membrane.

As reported previously, SPAK KO mice recapitulate many features that occur when NCC is disrupted genetically, either in mice or Gitelman patients. These features include hypokalemia, hypomagnesemia, and hypocalciuria (Schultheis et al., 1998; Simon et al., 1996). Hypokalemia is a cardinal feature of Gitelman syndrome; although the tendency for SPAK KO mice to be hypokalemic did not reach significance at baseline, moderate dietary potassium depletion led to greater hypokalemia in SPAK KO animals than in WT mice. Similarly, dietary $K^+$ depletion was required for NCC KO mice to develop hypokalemia (Morris et al., 2006; Schultheis et al., 1998). The trend to hypomagnesemia observed in the SPAK KO animals is likely the result of a deficiency in Trpm6, owing to atrophy or underdevelopment of the DCT, its predominant site of expression (Nijenhuis et al., 2005); it is also consistent with the observation that profound magnesium wasting does not typically occur when humans are treated with thiazide diuretics. Thiazides have not been reported to lead to distal atrophy when administered to humans (Ellison and Loffing, 2009). The observation that dietary NaCl loading did not normalize calcium excretion in SPAK KO animals supports the suggestion of Belge and colleagues (Belge et al., 2007) that both distal and proximal effects contribute to thiazide-induced hypocalciuria. Notably, the increased abundance of p-NKCC2 observed in the SPAK KO animals is mimicked by an increase in p-NKCC2 in NCC KO animals. Thus, in both cases (and, we presume, in patients with Gitelman syndrome), the tendency toward salt wasting is attenuated by activation of NKCC2 along the TAL.

Although the focus of the present work was not OSR1, the results do provide insight into the role of OSR1. OSR1 is expressed along both DCT and TAL, and differential OSR1 isoform expression was not detected. We have suggested that SPAK deletion activates NKCC2 by activating OSR1. Yet OSR1 is also expressed by DCT, whereas SPAK KO has the opposite effect. We suggest that the opposite effects reflect differing ratios of KS-SPAK to SPAK or OSR1 along TAL and DCT (also perhaps between medullary and cortical TAL segments). It is noteworthy, however, that SPAK deletion leads to the redistribution of OSR1 only along the DCT to a punctate, intracellular compartment. The functional consequences of this shift and of OSR1 in general have not been addressed directly because targeted disruption of OSR1 is embryonic lethal (Delpire and Gagnon, 2008), as is knockin of an inactivating T loop mutation (Rafiqi et al., 2010). Kidney-specific disruption of OSR1 will provide valuable insight into its role in ion homeostasis and blood pressure regulation.

In conclusion, the present data provide insight into the increasingly complex WNK-SPAK/OSR1-NCC/NKCC2 signaling complex in the kidney. They show that SPAK exerts substantial effects not only on NCC along the DCT, but also on NKCC2 along the TAL. They define an isoform switch, which should work to maintain homeostasis during ECF volume challenge by stimulating NaCl reabsorption along both segments by different mechanisms. The results also resolve a conundrum with respect to the divergent effects of SPAK KO and SPAK inactivation (Rodan and Huang, 2010). Finally, they provide support for the view that WNK signaling via SPAK/OSR1 to NCC/NKCC2 is neither unidirectional nor always stimulatory, but is instead highly recursive and tightly modulated, permitting mammals to tolerate diets that vary widely in $K^+$ and NaCl.

## EXPERIMENTAL PROCEDURES

### Animals

Animal studies were approved by the OHSU Institutional Animal Care and Usage Committee (Protocol A858). Generation of SPAK KO mice has been reported (Delpire and Gagnon, 2008). Briefly, the *SPAK* gene was disrupted by duplicating exon 6 and inserting tyrosinase, neomycin resistance, and 5′ hprt genes between the two exons. Animals carrying the mutant allele were identified by PCR genotyping of tail DNA, and final determination of genotype was performed by western blotting of kidney protein lysates following sacrifice.

### PCR Genotyping

Crude genomic DNA extracts were prepared from tail snips by heating at 95°C for 45 min in NaOH (pH 12.0), followed by neutralization with Tris-HCl (pH 5.0). To distinguish mice carrying at least one modified *SPAK* allele from WT mice, 4 μl of extract was used directly in PCR reactions as described (Delpire and Gagnon, 2008).

### Antibodies

The polyclonal NCC (Bostanjoglo et al., 1998), anti-NKCC2 (Schmitt et al., 2003), phospho-NKCC2 (Reiche et al., 2010), C-SPAK (Piechotta et al., 2002), p-T243SPAK/pT185OSR1 (purchased from Division of Signal Transduction Therapy, University of Dundee) (Rafiqi et al., 2010), pS71-NCC (Yang et al., 2007), and OSR1 (Zagórska et al., 2007) antibodies have all been published. The N-SPAK antibody was generated by ligating cDNA corresponding to amino acids 2–74 of mouse SPAK downstream of the GST open reading frame in the pGEX4 vector. The resulting fusion protein was injected into rabbits to produce polyclonal antibodies, and the antibody was purified by incubation with a GST fusion protein column at 4°C for 48 hr. After several washes, the antibody was eluted using 3 ml 100 mM Na-citrate (pH 2.5) and neutralized with 1.5 ml 1 M Tris-HCl (pH 8.5) and then dialyzed against 4 l of 1× PBS using a Spectra/Por 12,000–14,000 molecular weight cut-off (Spectrum Labs, Rancho Dominguez, CA). The affinity-purified antibody was then concentrated to a volume of 0.5–1 ml using a 15 ml 30,000 MWCO Amicon Ultra Centrifugal Filter device (Millipore, Danvers, MA). Finally, a small amount of BSA (1:400 dilution of 20 mg/ml) was added prior to freezing of aliquots at −20°C. This antibody recognized a band of the expected size in lysates from HEK293 cells (data not shown) and, importantly, on lysates from WT but not KO animals (see Figure 1D), indicating its high specificity for the N terminus of SPAK.

### Western Blot Analyses

Kidneys were removed, snap frozen in liquid nitrogen, and homogenized in chilled homogenization buffer containing protease and phosphatase inhibitors (50 mM Tris-HCl [pH 7.4], 1 mM EDTA, 1 mM EGTA, 0.3 M sucrose, 1 mM PMSF, 8.5 mM leupeptin, 1 mM orthovanadate, 50 mM Na fluoride, 1 mg/ml aprotinin, 1 mM dithiothreitol) on ice using a Potter Homogenizer. The homogenate was centrifuged at 4000× *g* for 15 min at 4°C, and the supernatant was separated on 3%–8% NuPage Tris acetate gel at 20 mA. Following transfer to PVDF membrane, equal loading was confirmed by staining the membrane with Ponceau red. Membranes were cut to allow parallel blotting with anti-β-actin to allow normalization. The blot was blocked with Blotto-T (5% nonfat dried milk in PBS-T) and incubated with the primary antibody for 1 hr, then washed and incubated with secondary antibody (HRP-coupled, diluted 1:4000, Zymed) and detected using the Western Lightning kit (Perkin Elmer). Densitometry using ImageJ software (NIH), normalized to β-actin, was performed to compare relative protein concentrations.

### 5′ RACE PCR and RT-PCR

5′ RACE PCR was performed using the SMARTer RACE cDNA Amplification Kit (Clontech) according to the manufacturer's protocol. Primers were: SPAKRACE6R, 5′ CCGTGTAACATCACCCCCTGTGGCTAAG; SPAKRACE10R, 5′CCTTCTTGGCTCTTTGGGCTATGTCTGGGG. PCR products were A-tailed and cloned in pGEM-T Easy (Promega), and minipreps were sequenced. To determine tissue expression of exon 5a-containing transcripts, RT-PCR was performed using primers against exon 5a (see Figure S1) and SPAKRACE10R with multitissue panel I (Clontech, Palo Alto, CA) as template. For brain, which is not part of cDNA panel I, total RNA from mouse brain was isolated and used in PCR following reverse transcription.

### In Vitro Kinase Assay

GST fusion proteins were made by subcloning mouse-derived fragments into pGex6P-1, followed by induction of protein expression in BL21 cells (Novagen); the GST moiety was cleaved using PreScission Protease (GE Healthcare). In vitro kinase assays were performed by combining in a 30 μl reaction 1 μg of NCC N2-142 or NKCC2 N2-172 and 0.5 μg of a constitutively active mutant of SPAK (T243E) or OSR1 (T185E) with 0.4, 1.2, 2.4, or 4.8 μg KS-SPAK in kinase assay buffer (10 mM HEPES [pH 8.0], 10 mM $MgCl_2$, 2 mM benzamidine, 2 mM DTT) with 0.15 mM cold ATP and 10 μCi ATP $\gamma$-$^{32}$P. Reactions were incubated at 30°C for 45 min, then stopped by adding SDS-PAGE sample buffer and boiling for 5 min at 100°C. Samples were then resolved on 4%–12% Bis-tris polyacrylamide gels, Coomassie stained, dried, and exposed to autoradiographic film.

### NCC Phosphorylation in HEK293 Cells

All plasmids were generated by cloning cDNAs into pMO-myc, which uses the SV40 promoter to drive expression in mammalian cells. HEK293 cells were plated at a density of $1.75 \times 10^5$ cells/well in 12-well plates. The next day, cells were transfected with 0.25 μg mouse NCC and increasing amounts of mouse KS-SPAK (0, 1, 1.5, 2.5, or 5 μg) using calcium phosphate precipitation. Medium was changed 24 hr later, and cells were harvested in lysis buffer 48 hr posttransfection for western blotting.

### Blood Pressure Measurement

Blood pressures were measured using CODA-6 tail cuff blood pressure monitoring system (Kent Scientific). The mice were trained prior to the studies by restraint with 25 cycles of cuff inflation/deflation on 5 consecutive days. On subsequent days, measurements were made after 5 min of restraint with no external manipulation or stimulation. Ten acclimation cycles, followed by fifteen measurement cycles, were performed. Blood pressure measurements were done for 5 consecutive days on alternating channels of the CODA-6. When dietary changes were made, 14 days were allowed to pass before measurements were made. During this time, the blood pressures were measured 5 days a week to keep mice acclimated to the procedure, but the data were discarded.

### Diuretic Response

Diuretic responses were determined using a method previously reported. Mice maintained on 0.49% NaCl control diet had their bladders emptied via manual massage. Mice were then placed in metabolic cages, and urine was then collected under water-saturated light mineral oil for 3 hr. Furosemide or HCTZ (dissolved in 1.7% ethanolamine) was injected intraperitoneally at 25 mg/kg, and a further 3 hr urine collection was performed. Urinary sodium and creatinine levels were then assayed as described below.

### Analysis of Blood Electrolytes

Whole blood was collected via lateral saphenous vein sampling or terminal cardiac puncture (under anesthesia) and placed into heparinized Eppendorf tubes. One hundred microliters of whole blood was then immediately added to a Chem8 cartridge, or 65 μl was added to E3 cartridge and analyzed using i-STAT analyzer (Abbot Point of Care, Inc.). Plasma magnesium was measured by a colorimetric assay (Pointe Scientific).

### Plasma Aldosterone and Renin Activity

Plasma aldosterone levels were measured by ELISA (IBL-America). PRA was measured as the amount of angiotensin I generated after incubation with excess angiotensinogen (MP Biomedicals). Two microliters of plasma were incubated with excess porcine angiotensinogen (4 μM) in a 10 μl reaction containing sodium acetate (50 mM, pH 6.5), AEBSF (2.5 mM), 8-hydroxyquinoline (1 mM), and EDTA (5 mM) for 15 min at 37°C. The assay was linear for at least 30 min. The reaction was stopped by boiling for 5 min and diluted 1:50, and angiotensin I was measured by ELISA (Phoenix Pharmaceuticals).

### Analysis of Urine

For calcium determination, spot urine samples were collected by placing mice in a clean metabolic cage until the mice spontaneously voided. Urinary calcium was measured by o-Cresolphthalein Complexone method (Pointe Scientific), according to the manufacturer's protocol, except that samples were diluted 1:2. Urinary creatinine was measured by modified Jaffe method (Pointe Scientific) on samples diluted 1:10. Urinary calcium:creatinine ratios were calculated from this data. Urinary sodium in samples obtained in the diuretic response study was measured by flame photometry.

### Dietary Manipulation

Custom research diets with varying NaCl levels (0.01%, 0.49%, and 8% NaCl) and potassium-deficient diet (Harlan Teklad) were used. Mice aged 3–4 months were placed on control diet (0.49% NaCl, 0.8% $K^+$) or NaCl-deficient diet and subjected to blood pressure, urinary, and plasma electrolyte analysis. The diet was then changed to the other diet, and blood pressure, urinary, and plasma electrolyte analysis was performed after 7–14 days, followed by harvesting of kidneys. Mice were placed on high-NaCl diet for 2 weeks, and spot urine was collected, followed by cardiac puncture with electrolyte analysis and harvesting of kidneys.

### Immunofluorescence

Mice were anesthetized and kidneys perfusion-fixed by retrograde abdominal aortic perfusion of 3% paraformaldehyde in PBS (pH 7.4). After cryoprotection with 30% sucrose and freezing, 5 μm sections were cut, washed in 1× PBS ×3, incubated in 1× PBS with 0.5%Triton X for 30 min, washed in PBS, and blocked in 5% milk in PBS for 1 hr. Primary antibody (1:500) in 5% milk in 1× PBS was added for 1 hr, followed by a wash in PBS. Sections were incubated for 1 hr with 1:500 FITC-conjugated secondary antibody (Zymed) in block, then washed.

### Morphometric Procedures

The fractional volume of DCT segments among strains was measured by light microscopy according to previously characterized methods (Ellison et al., 1989). Briefly, 5 μm-thick paraffin sections were stained for NCC to identify DCT. Cortical areas extending between the renal capsule and the outer medullary boundary were evaluated. Sections were photographed and printed at a final magnification of ×100. At least five prints per animal were evaluated.

### Statistical Analyses

Data were analyzed using SPSS (Version 17.0, Chicago, IL). All values are expressed as means ± standard error of the mean. If a Kolmogorov-Smirnov test indicated that data were normally distributed, data were analyzed using analysis of variance (ANOVA) and, if significant, a least-significant-difference post

hoc test. Alternatively, data were analyzed using a Kruskal-Wallis (nonparametric) test or a Mann-Whitney U test, as indicated in the figure legends.

## SUPPLEMENTAL INFORMATION

Supplemental Information includes five figures and two tables and can be found with this article online at doi:10.1016/j.cmet.2011.07.009.

## ACKNOWLEDGMENTS

This work was supported by grants from the NIH (K01 DK076617 to J.A.M. and DK51496 to D.H.E.), the Department of Veterans Affairs (Merit Review to D.H.E.), and the American Heart Association (to D.H.E.). E.J.H. is supported by an Erasmus MC Fellowship and by the Dutch Kidney Foundation (KJPB 08.004). J.H.N was supported by NIDDK 1T32 DK067864. Prior support from the American Society of Nephrology to D.H.E. is also acknowledged. We also acknowledge Nicole Desmarais for technical assistance.

Received: February 25, 2011
Revised: June 9, 2011
Accepted: July 29, 2011
Published: September 6, 2011

## REFERENCES

Anselmo, A.N., Earnest, S., Chen, W., Juang, Y.C., Kim, S.C., Zhao, Y., and Cobb, M.H. (2006). WNK1 and OSR1 regulate the Na+, K+, 2Cl- cotransporter in HeLa cells. Proc. Natl. Acad. Sci. USA *103*, 10883–10888.

Belge, H., Gailly, P., Schwaller, B., Loffing, J., Debaix, H., Riveira-Munoz, E., Beauwens, R., Devogelaer, J.P., Hoenderop, J.G., Bindels, R.J., and Devuyst, O. (2007). Renal expression of parvalbumin is critical for NaCl handling and response to diuretics. Proc. Natl. Acad. Sci. USA *104*, 14849–14854.

Bostanjoglo, M., Reeves, W.B., Reilly, R.F., Velázquez, H., Robertson, N., Litwack, G., Morsing, P., Dørup, J., Bachmann, S., and Ellison, D.H. (1998). 11Beta-hydroxysteroid dehydrogenase, mineralocorticoid receptor, and thiazide-sensitive Na-Cl cotransporter expression by distal tubules. J. Am. Soc. Nephrol. *9*, 1347–1358.

Delpire, E., and Gagnon, K.B. (2008). SPAK and OSR1: STE20 kinases involved in the regulation of ion homoeostasis and volume control in mammalian cells. Biochem. J. *409*, 321–331.

Dowd, B.F., and Forbush, B. (2003). PASK (proline-alanine-rich STE20-related kinase), a regulatory kinase of the Na-K-Cl cotransporter (NKCC1). J. Biol. Chem. *278*, 27347–27353.

Ellison, D.H., and Loffing, J. (2009). Thiazide effects and adverse effects: insights from molecular genetics. Hypertension *54*, 196–202.

Ellison, D.H., Velázquez, H., and Wright, F.S. (1989). Adaptation of the distal convoluted tubule of the rat. Structural and functional effects of dietary salt intake and chronic diuretic infusion. J. Clin. Invest. *83*, 113–126.

Feng, M., Whitesall, S., Zhang, Y., Beibel, M., D'Alecy, L., and DiPetrillo, K. (2008). Validation of volume-pressure recording tail-cuff blood pressure measurements. Am. J. Hypertens. *21*, 1288–1291.

Geng, Y., Byun, N., and Delpire, E. (2010). Behavioral analysis of Ste20 kinase SPAK knockout mice. Behav. Brain Res. *208*, 377–382.

Glover, M., Zuber, A.M., and O'Shaughnessy, K.M. (2009). Renal and brain isoforms of WNK3 have opposite effects on NCCT expression. J. Am. Soc. Nephrol. *20*, 1314–1322.

Hadchouel, J., Soukaseum, C., Büsst, C., Zhou, X.O., Baudrie, V., Zürrer, T., Cambillau, M., Elghozi, J.L., Lifton, R.P., Loffing, J., and Jeunemaitre, X. (2010). Decreased ENaC expression compensates the increased NCC activity following inactivation of the kidney-specific isoform of WNK1 and prevents hypertension. Proc. Natl. Acad. Sci. USA *107*, 18109–18114.

Lazrak, A., Liu, Z., and Huang, C.L. (2006). Antagonistic regulation of ROMK by long and kidney-specific WNK1 isoforms. Proc. Natl. Acad. Sci. USA *103*, 1615–1620.

Lee, D.H., Riquier, A.D., Yang, L.E., Leong, P.K., Maunsbach, A.B., and McDonough, A.A. (2009). Acute hypertension provokes acute trafficking of distal tubule Na-Cl cotransporter (NCC) to subapical cytoplasmic vesicles. Am. J. Physiol. Renal Physiol. *296*, F810–F818.

Liu, Z., Wang, H.R., and Huang, C.L. (2009). Regulation of ROMK channel and K+ homeostasis by kidney-specific WNK1 kinase. J. Biol. Chem. *284*, 12198–12206.

Mayan, H., Vered, I., Mouallem, M., Tzadok-Witkon, M., Pauzner, R., and Farfel, Z. (2002). Pseudohypoaldosteronism type II: marked sensitivity to thiazides, hypercalciuria, normomagnesemia, and low bone mineral density. J. Clin. Endocrinol. Metab. *87*, 3248–3254.

Morris, R.G., Hoorn, E.J., and Knepper, M.A. (2006). Hypokalemia in a mouse model of Gitelman's syndrome. Am. J. Physiol. Renal Physiol. *290*, F1416–F1420.

Mutig, K., Saritas, T., Uchida, S., Kahl, T., Borowski, T., Paliege, A., Böhlick, A., Bleich, M., Shan, Q., and Bachmann, S. (2010). Short-term stimulation of the thiazide-sensitive Na+-Cl- cotransporter by vasopressin involves phosphorylation and membrane translocation. Am. J. Physiol. Renal Physiol. *298*, F502–F509.

Nijenhuis, T., Vallon, V., van der Kemp, A.W., Loffing, J., Hoenderop, J.G., and Bindels, R.J. (2005). Enhanced passive Ca2+ reabsorption and reduced Mg2+ channel abundance explains thiazide-induced hypocalciuria and hypomagnesemia. J. Clin. Invest. *115*, 1651–1658.

Piechotta, K., Lu, J., and Delpire, E. (2002). Cation chloride cotransporters interact with the stress-related kinases Ste20-related proline-alanine-rich kinase (SPAK) and oxidative stress response 1 (OSR1). J. Biol. Chem. *277*, 50812–50819.

Piechotta, K., Garbarini, N., England, R., and Delpire, E. (2003). Characterization of the interaction of the stress kinase SPAK with the Na+-K+-2Cl- cotransporter in the nervous system: evidence for a scaffolding role of the kinase. J. Biol. Chem. *278*, 52848–52856.

Rafiqi, F.H., Zuber, A.M., Glover, M., Richardson, C., Fleming, S., Jovanović, S., Jovanović, A., O'Shaughnessy, K.M., and Alessi, D.R. (2010). Role of the WNK-activated SPAK kinase in regulating blood pressure. EMBO Mol. Med. *2*, 63–75.

Reiche, J., Theilig, F., Rafiqi, F.H., Carlo, A.S., Militz, D., Mutig, K., Todiras, M., Christensen, E.I., Ellison, D.H., Bader, M., et al. (2010). SORLA/SORL1 functionally interacts with SPAK to control renal activation of Na(+)-K(+)-Cl(-) cotransporter 2. Mol. Cell. Biol. *30*, 3027–3037.

Richardson, C., and Alessi, D.R. (2008). The regulation of salt transport and blood pressure by the WNK-SPAK/OSR1 signalling pathway. J. Cell Sci. *121*, 3293–3304.

Richardson, C., Sakamoto, K., de los Heros, P., Deak, M., Campbell, D.G., Prescott, A.R., and Alessi, D.R. (2011). Regulation of the NKCC2 ion cotransporter by SPAK-OSR1-dependent and -independent pathways. J. Cell Sci. *124*, 789–800.

Rodan, A.R., and Huang, C.L. (2010). An emerging role for SPAK in NCC, NKCC, and blood pressure regulation. J. Am. Soc. Nephrol. *21*, 1812–1814.

Sandberg, M.B., Maunsbach, A.B., and McDonough, A.A. (2006). Redistribution of distal tubule Na+-Cl- cotransporter (NCC) in response to a high-salt diet. Am. J. Physiol. Renal Physiol. *291*, F503–F508.

Sandberg, M.B., Riquier, A.D., Pihakaski-Maunsbach, K., McDonough, A.A., and Maunsbach, A.B. (2007). ANG II provokes acute trafficking of distal tubule Na+-Cl(-) cotransporter to apical membrane. Am. J. Physiol. Renal Physiol. *293*, F662–F669.

Schmitt, R., Klussmann, E., Kahl, T., Ellison, D.H., and Bachmann, S. (2003). Renal expression of sodium transporters and aquaporin-2 in hypothyroid rats. Am. J. Physiol. Renal Physiol. *284*, F1097–F1104.

Schultheis, P.J., Lorenz, J.N., Meneton, P., Nieman, M.L., Riddle, T.M., Flagella, M., Duffy, J.J., Doetschman, T., Miller, M.L., and Shull, G.E. (1998). Phenotype resembling Gitelman's syndrome in mice lacking the apical Na+-Cl- cotransporter of the distal convoluted tubule. J. Biol. Chem. *273*, 29150–29155.

Simon, D.B., Nelson-Williams, C., Bia, M.J., Ellison, D., Karet, F.E., Molina, A.M., Vaara, I., Iwata, F., Cushner, H.M., Koolen, M., et al. (1996). Gitelman's variant of Bartter's syndrome, inherited hypokalaemic alkalosis, is caused by mutations in the thiazide-sensitive Na-Cl cotransporter. Nat. Genet. *12*, 24–30.

Subramanya, A.R., Yang, C.L., Zhu, X., and Ellison, D.H. (2006). Dominant-negative regulation of WNK1 by its kidney-specific kinase-defective isoform. Am. J. Physiol. Renal Physiol. *290*, F619–F624.

van der Lubbe, N., Lim, C.H., Fenton, R.A., Meima, M.E., Jan Danser, A.H., Zietse, R., and Hoorn, E.J. (2011). Angiotensin II induces phosphorylation of the thiazide-sensitive sodium chloride cotransporter independent of aldosterone. Kidney Int. *79*, 66–76.

Vitari, A.C., Deak, M., Morrice, N.A., and Alessi, D.R. (2005). The WNK1 and WNK4 protein kinases that are mutated in Gordon's hypertension syndrome phosphorylate and activate SPAK and OSR1 protein kinases. Biochem. J. *391*, 17–24.

Wade, J.B., Fang, L., Liu, J., Li, D., Yang, C.L., Subramanya, A.R., Maouyo, D., Mason, A., Ellison, D.H., and Welling, P.A. (2006). WNK1 kinase isoform switch regulates renal potassium excretion. Proc. Natl. Acad. Sci. USA *103*, 8558–8563.

Welker, P., Böhlick, A., Mutig, K., Salanova, M., Kahl, T., Schlüter, H., Blottner, D., Ponce-Coria, J., Gamba, G., and Bachmann, S. (2008). Renal Na+-K+-Cl- cotransporter activity and vasopressin-induced trafficking are lipid raft-dependent. Am. J. Physiol. Renal Physiol. *295*, F789–F802.

Wilson, F.H., Disse-Nicodème, S., Choate, K.A., Ishikawa, K., Nelson-Williams, C., Desitter, I., Gunel, M., Milford, D.V., Lipkin, G.W., Achard, J.M., et al. (2001). Human hypertension caused by mutations in WNK kinases. Science *293*, 1107–1112.

Yang, S.S., Morimoto, T., Rai, T., Chiga, M., Sohara, E., Ohno, M., Uchida, K., Lin, S.H., Moriguchi, T., Shibuya, H., et al. (2007). Molecular pathogenesis of pseudohypoaldosteronism type II: generation and analysis of a Wnk4(D561A/+) knockin mouse model. Cell Metab. *5*, 331–344.

Yang, S.S., Lo, Y.F., Wu, C.C., Lin, S.W., Yeh, C.J., Chu, P., Sytwu, H.K., Uchida, S., Sasaki, S., and Lin, S.H. (2010). SPAK-knockout mice manifest Gitelman syndrome and impaired vasoconstriction. J. Am. Soc. Nephrol. *21*, 1868–1877.

Zagórska, A., Pozo-Guisado, E., Boudeau, J., Vitari, A.C., Rafiqi, F.H., Thastrup, J., Deak, M., Campbell, D.G., Morrice, N.A., Prescott, A.R., and Alessi, D.R. (2007). Regulation of activity and localization of the WNK1 protein kinase by hyperosmotic stress. J. Cell Biol. *176*, 89–100.